JACS
JOURNAL OF THE AMERICAN CHEMICAL SOCIETY
Article
pubs.acs.org/JACS

Effect of Backbone Flexibility on Charge Transfer Rates in Peptide Nucleic Acid Duplexes

Emil Wierzbinski,[†] Arnie de Leon,[‡] Xing Yin,[†] Alexander Balaeff,[§] Kathryn L. Davis,[†] Srinivas Reppireddy,[‡] Ravindra Venkatramani,[§] Shahar Keinan,[§] Danith H. Ly,[‡] Marcela Madrid,[⊥] David N. Beratan,*[,∥] Catalina Achim,*[,‡] and David H. Waldeck*[,†]

[†]Department of Chemistry, University of Pittsburgh, Pittsburgh, Pennsylvania 15260, United States
[‡]Department of Chemistry, Carnegie Mellon University, Pittsburgh, Pennsylvania 15213, United States
[§]Department of Chemistry, Duke University, Durham, North Carolina 27708, United States
[⊥]Pittsburgh Supercomputing Center, Pittsburgh, Pennsylvania 15213, United States
[∥]Departments of Chemistry, Biochemistry, and Physics, Duke University, Durham, North Carolina 27708, United States

Supporting Information

ABSTRACT: Charge transfer (CT) properties are compared between peptide nucleic acid structures with an aminoethylglycine backbone (aeg-PNA) and those with a γ-methylated backbone (γ-PNA). The common aeg-PNA is an achiral molecule with a flexible structure, whereas γ-PNA is a chiral molecule with a significantly more rigid structure than aeg-PNA. Electrochemical measurements show that the CT rate constant through an aeg-PNA bridging unit is twice the CT rate constant through a γ-PNA bridging unit. Theoretical calculations of PNA electronic properties, which are based on a molecular dynamics structural ensemble, reveal that the difference in the CT rate constant results from the difference in the extent of backbone fluctuations of aeg- and γ-PNA. In particular, fluctuations of the backbone affect the local electric field that broadens the energy levels of the PNA nucleobases. The greater flexibility of the aeg-PNA gives rise to more broadening, and a more frequent appearance of high-CT rate conformations than in γ-PNA.

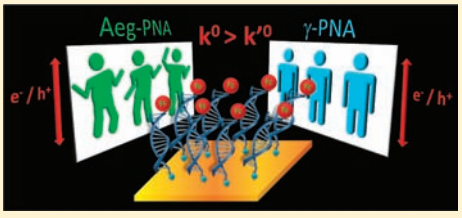

INTRODUCTION

DNA and its synthetic analogues are of great interest because of their potential applications as scaffolds for nanostructures[1] and as active elements in nanoelectronic devices.[1c,2] In part, this promise arises from the fact that nucleic acids (NAs) can form well-defined, supramolecular structures based on Watson–Crick hybridization. Our interest lies in the long-distance charge transfer (CT) properties of NAs and the dependence of these properties on nucleobase sequence and on the backbone chemical structure.[3] While the nucleobase effect on CT in NAs is widely explored, the impact of the backbone's properties on the CT is not as well studied.[4] It has been shown in theoretical investigations[4a] that the CT efficiency of DNA and peptide nucleic acid (PNA) with identical base pair (bp) sequence can be different, and the CT properties are dependent on the structural fluctuations in these fragments. This work explores how the backbone rigidity affects the CT properties of NAs.

Several CT mechanisms are known to operate in NAs (see ref 5 and references therein). In the short distance range, the CT is characterized by an exponential decrease of the rate constant with distance and is commonly understood to follow a superexchange dominated tunneling mechanism. Across longer distances, the thermally-induced hopping mechanism is assumed to operate, wherein the CT rate constant decreases as a power law. In addition to the distance, the CT mechanism depends on the NA sequence and the energy levels of the charge donor and acceptor (or the electrode Fermi energy). In certain situations, a near-resonant CT regime was identified, wherein the hopping and superexchange CT mechanisms coexist.[6]

The effect of the nucleobase sequence on hole localization and transport is strongly correlated with the presence of guanine (G).[7] Because of its lower oxidation potential with respect to the other nucleobases, G can stabilize positive charges (holes) and thus dominates the CT mechanism.[8] The charge transport through DNA can also be accelerated by replacing adenine (A) in thymine-adenine (TA) base pairs by a lower oxidation potential base, such as 7-deazaadenine[7e] or diaminopurine.[7d,e] It is important to note that clusters of such bases do not accelerate the overall hole transport.[9] For example, Sugiyama and co-workers showed that adjacent G bases, GG or GGG, do not cause an increase in the rate constant of long-range CT through DNA, but can act as hole trapping states.[10] Electronic structure calculations suggest that CT may be enhanced by extending the aromaticity of the nucleobases, as in size-extended DNA.[11] Another strategy to manipulate the charge transport in NAs is to incorporate metal ions into the NA helix, resulting in the so-called M-DNA.[12] Finally, we note that CT through DNA can be significantly perturbed by

Received: March 1, 2012
Published: April 30, 2012

   dx.doi.org/10.1021/ja301677z | J. Am. Chem. Soc. 2012, 134, 9335–9342

"defects", such as bp mismatches,[13] abasic sites,[13b] and methylated or oxidized nucleobases.[14]

While earlier CT studies of NAs showed unequivocally that the nucleobase sequence is a major determinant of the mechanism and the CT rate, the influence of the NA backbone on CT is relatively poorly studied.[4] For example, Barton et al. showed that CT through DNA monolayers was not affected by a nick in the DNA backbone.[4b] However, other studies found that the nucleobase geometry and fluctuations, which are determined by the NA backbone chemistry, have a noticeable effect on the CT rate and mechanism in NAs. For example, a theoretical study by Hatcher et al.[4a] concluded that the CT through 4-bp-long DNA and PNA[15] duplexes was affected by the structural flexibility of the duplexes. In particular, the CT rate constant through PNA was predicted to be larger than that through DNA because larger fluctuations make PNA more likely to adopt conformations with stronger donor−acceptor couplings that favor CT. Notably, Hatcher et al. focused on hole mediation by the nucleobase stack only; the NA backbone was included in their geometry sampling but not in their quantum mechanical analysis of CT. This approximation has been standard in treating the NA electronic structure because the ground and the first excited states of the excess charge are localized mostly on the nucleobases.[4a,5,16]

DNA analogues enable investigations of how the backbone structure and dynamics can affect the CT rate through NAs. A wide variety of NA structures, such as locked nucleic acid (LNA),[17] threose nucleic acid (TNA),[18] glycol nucleic acid (GNA),[19] and PNA[20] are available. Although these analogues hybridize according to the Watson−Crick rules, their helicoidal parameters and their conformational flexibility vary. Consequently, the electronic couplings among bases in different analogues of DNA vary as well. Additionally, the NA backbone structure and fluctuations affect those of the nucleobase stack and may have a gating effect on the CT through the nucleobases, as has been reported for DNA[21] and other molecules.[22] Apart from the direct conformational effect, the differences in the backbone structure and chemical composition between the NAs translate into differences in local electric field that the nucleobases experience. Hence, the polarization and broadening of nucleobase-localized charge states differ among the NAs, resulting in different CT properties.[16a]

This study uses two different forms of ds PNA, aeg- and γ-methylated, to investigate how the backbone can affect charge transport, and hence the observed CT rate. Typically, the backbone of PNA is based on the neutral and achiral 2-aminoethylglycine (aeg),[23] which is more flexible than the DNA backbone constrained by ribose rings and stiffened by the phosphates' charges.[24] Indeed, the aeg-PNA is an achiral molecule capable of adopting both a right- and a left-handed helical conformation. Incorporation of side chains at the γ position of the backbone, for example, the γ-methylation studied here, locks the molecule in a single chiral state and makes the γ-PNA more rigid than aeg-PNA (Figure 1).[20b,25] Consequently, hybrid duplexes PNA/DNA and PNA/RNA,[23a,b] and PNA/PNA duplexes that contain γ-PNA strands have greater thermal stability than the corresponding duplexes containing aeg-PNA strands.[23c] Comparison of the CT rate and mechanism between the aeg- and γ-PNA provides an excellent way to study the relationship between molecular CT and molecular fluctuations and chirality.

Using the same methodology as in earlier work,[6,26] this study examined the oxidation and reduction of a ferrocene moiety (Fc) which was attached to a terminus of the PNA molecules assembled into a monolayer on a gold electrode. Cyclic voltammetry data were fitted by Marcus theory and used to determine the standard heterogeneous rate constant k^0.[27] The key finding of this study is that the electrochemical CT rate constants for γ-PNA duplexes are lower than those for aeg-PNA duplexes.

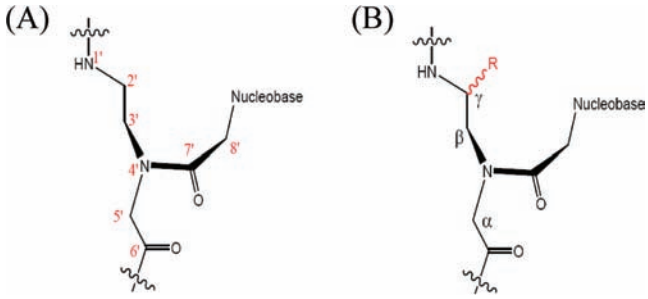

Figure 1. (A) Chemical structure of the backbone of aeg-PNA. (B) Chemical structure of the γ-PNA. In this study, R = methyl.

RESULTS AND DISCUSSION

The CT properties of two different 7-bp ds PNAs were investigated: one ds PNA contained only TA base pairs while the other contained a central GC base pair (Table 1).

Table 1. Sequences and Functional Groups of PNA Duplexes[a]

Abbreviation	Sequence
aeg -$PNA_{(TA)}$ / γ -$PNA_{(TA)}$	Cys-T_3-**T**-T_3-Fc A_3-**A**-A_3-Lys
aeg -$PNA_{(GC)}$ / γ-$PNA_{(GC)}$	Cys-T_3-**G**-T_3-Fc A_3-**C**-A_3-Lys

[a]The PNAs were assembled on gold electrodes via a C-terminal cysteine (Cys) group. The N-terminal ferrocene served as the redox reporter group.

Surface coverage and thickness data for the PNA films are presented in Table 2. Self-assembled monolayers (SAMs) of Fc-terminated PNA molecules were adsorbed on gold electrodes as described in the Methods section below (cf. refs 6 and 26b). The surface coverage of the SAMs was determined from the total amount of charge transferred, which was obtained by integrating the area of the Faradaic current peaks (Figure 2B−D). The surface coverage of aeg- and γ-PNA SAMs are similar and indicate that both PNAs form densely packed monolayers on Au (Table 2). This observation was confirmed by ellipsometry measurements of the PNA film thickness (see Table 2), which was found to be comparable to the thickness of 7-bp aeg-PNA monolayers reported earlier.[6,26c]

Figure 2 shows representative cyclic voltammograms for SAMs of ds aeg-PNA and γ-PNA. Analysis of the voltammograms shows that the Fc redox couple is quasi-reversible. The relationship between the shift of the oxidation/reduction peak potential from the formal potential of the Fc ($E_p - E^0$) and the scan rate can be described by Marcus theory, as was found in prior studies.[6,26] Because the Fc groups are significantly smaller than the ds-PNA, interactions between them are weak and do not affect the redox reaction significantly (see refs 6 and 26).

dx.doi.org/10.1021/ja301677z | J. Am. Chem. Soc. 2012, 134, 9335−9342

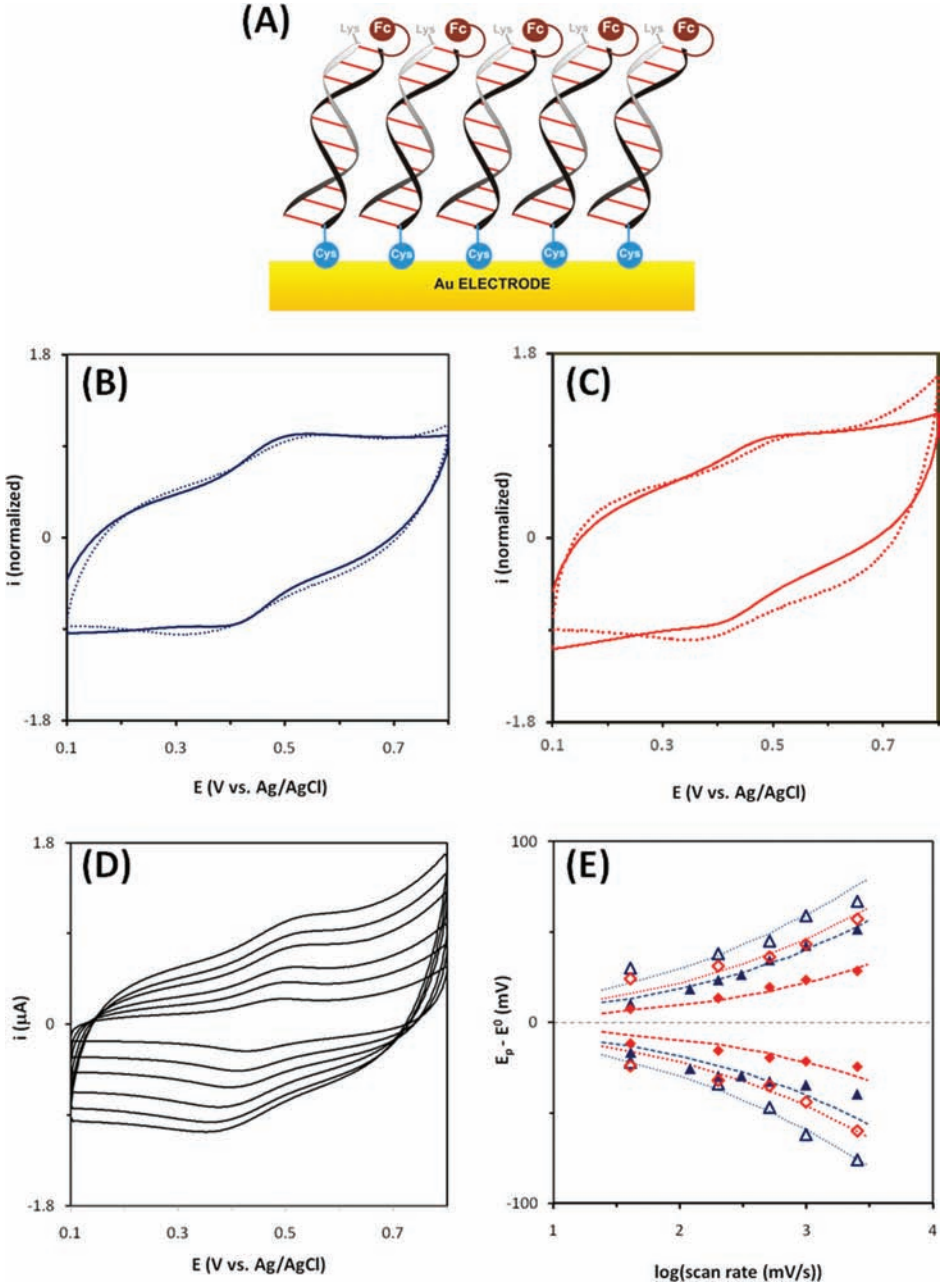

Figure 2. (A) Schematic representation of Fc-terminated PNA SAMs on gold electrodes used for electrochemical studies. (B) Voltammograms (normalized to the anodic peak current) taken at 30 mV/s for SAMs of aeg-$PNA_{(TA)}$ (blue, solid) and γ-$PNA_{(TA)}$ (blue, dashed) on gold electrodes. (C) Voltammograms (normalized to the anodic peak current) taken at 30 mV/s for SAMs of aeg-$PNA_{(GC)}$ (red, solid), and γ-$PNA_{(GC)}$ (red, dashed) on gold electrodes. (D) Voltammograms (non-normalized current) for a SAM of γ-$PNA_{(GC)}$ taken at scan rates from 5 to 30 mV/s (with 5 mV/s increment). (E) Peak position relative to the formal potential ($E_p - E^0$) versus log (scan rate) for aeg- (filled symbols) and γ- (open symbols) $PNA_{(TA)}$ (blue triangles), and $PNA_{(GC)}$ (red diamonds) sequences, with corresponding Marcus theory fits: aeg- (dashed blue) and γ- (dotted blue) $PNA_{(TA)}$, and aeg- (dashed red) and γ- (dotted red) $PNA_{(GC)}$.

Table 2. Electrochemical CT Rate Constant k^0, Surface Coverage, and Thickness of the Ferrocene-Terminated PNA Films

sequence	k^0/s^{-1}	coverage/pmol cm^{-2}	film thickness/nm
aeg-$PNA_{(TA)}$	0.25 ± 0.05	110 ± 40	2.8 ± 0.6
γ-$PNA_{(TA)}$	0.11 ± 0.06	68 ± 21	2.8 ± 0.7
aeg-$PNA_{(GC)}$	0.57 ± 0.14	120 ± 50	3.5 ± 0.2
γ-$PNA_{(GC)}$	0.22 ± 0.07	86 ± 27	3.0 ± 0.4

The average standard heterogeneous rate constants determined for the ds PNA SAMs are presented in Table 2.

The data in Table 2 reveal two clear trends. First, replacement of a central TA base pair with a GC base pair causes an increase in the CT rate constant for both aeg- and γ-PNA by a factor of about two. This effect demonstrates the sensitivity of the CT kinetics to the nucleobase identity: G has a lower oxidation potential than A; therefore, a GC pair presents a lower hole tunneling barrier than an AT pair.[8] Second, comparison of the rate constants for duplexes of the same sequence but different backbone chemistry shows that a change

dx.doi.org/10.1021/ja301677z | J. Am. Chem. Soc. 2012, 134, 9335−9342

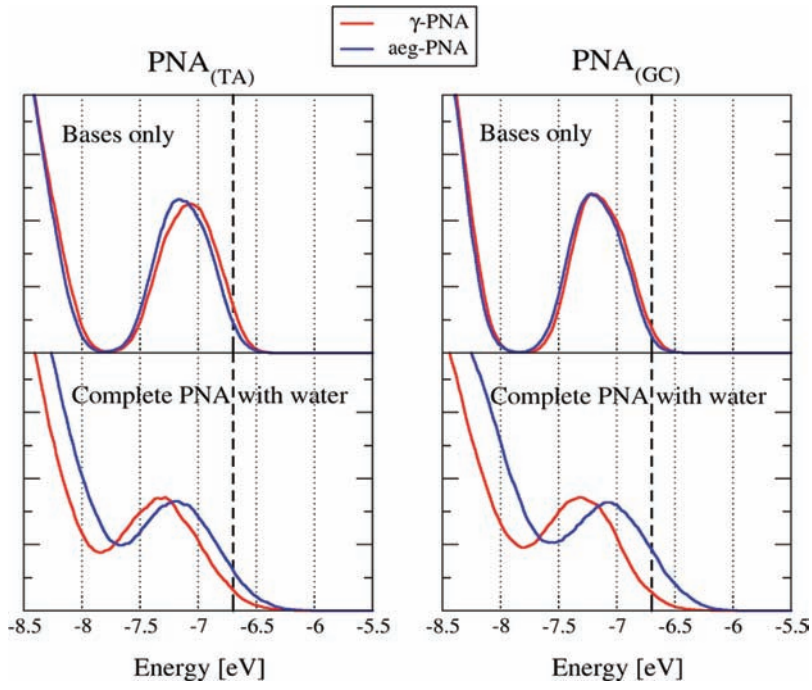

Figure 3. Electronic density of states (DOS) computed for the MD ensembles of the four studied PNA systems. Top row: DOS computed for nucleobases only. Bottom row: DOS computed for both bases and backbone, with the water included as point charges to account for the solvent screening of electrostatic interactions. The proximity of the DOS peaks to the Fermi level −6.7 eV, identified by the vertical dashed lines, puts the systems into a near-resonant regime.[6].

from the aeg-backbone to the γ-methylated backbone attenuates the CT rate constant by about a factor of 2 (Table 2). This effect is new, and its origin is not immediately evident. Thus the central question of this manuscript arises: Why does the chemical change in the backbone cause the CT rate constant to change?

Several explanations can be ruled out. First, methylation of the backbone does not have a significant effect on the average geometry of the nucleobase stack, to which the CT rate is highly sensitive. Indeed, molecular dynamics (MD) simulations employing NMR constraints indicate that γ-PNA adopts a general P-form helical structure that is very similar to the well documented structure of aeg-PNA.[25] Next, we can rule out the backbone effect on the structure of the PNA film. Because the CT rate constant measurements were performed on molecular monolayers, the number of molecules and their arrangement in the SAMs might be expected to influence the overall CT rate constant. For example, CT in low-coverage films can be conformationally gated by bending of the DNA or PNA strand toward the electrode surface;[28] however, such motions are disfavored in the closely packed PNA films used here (see Table 2).[6,26] Besides, the trend in observed electrochemical CT rate with the measured PNA surface coverages (Table 2) is opposite to that expected for gating by large-scale molecular motions, i.e., the more densely packed films exhibit higher CT rates even though the large-amplitude molecular motions in those films are suppressed. Finally, the dependence of the rate constant on the PNA sequence provides another argument in favor of bridge-mediated CT, as opposed to direct CT gated by PNA bending motions. Thus, we are left to consider the influence of the backbone on the PNA structural fluctuations.

Appreciation of the importance of conformational fluctuations on CT kinetics and mechanism in NAs and proteins has been growing.[5,16b,29] An important difference between aeg-PNA and γ-PNA is the extent of structural fluctuations and their impact on the conformational ensemble of the nucleobase stack. It is possible that aeg-PNA more often populates well-coupled, high-conductance conformations of the base pairs than does γ-PNA, because aeg-PNA adopts a broader range of conformations than γ-PNA. Although it is possible that the broader range of conformations includes low-conductance conformations; for NAs, the increased fluctuations have been shown to lead only to an increase in molecular CT rate. A computational study of 4-bp, palindromic fragments of DNA and PNA[4a] found that both the donor−acceptor coupling and the bridge hopping probability in NAs is linked to conformational flexibility. That result is consistent with the current experimental findings that the more flexible aeg-PNA has a larger CT rate constant than the more rigid γ-methylated PNA (Table 2).

In order to test the hypothesis that structural fluctuations affect the CT rate, computational studies of PNA were performed according to a protocol established previously (see the Methods section for details).[6,26b] The MD simulations confirmed the *a priori* expectation that the flexibility and fluctuations of γ-PNA are smaller than those of aeg-PNA. For instance, the root-mean-square deviation (rmsd) of the aeg-PNA structure from its average structure is 25−30% larger than that found for γ-PNA (1.11 ± 0.19 Å for aeg-$PNA_{(TA)}$ versus 0.81 ± 0.15 Å for γ-$PNA_{(TA)}$, and 1.17 ± 0.27 Å for aeg-$PNA_{(GC)}$ versus 0.80 ± 0.17 Å for γ-$PNA_{(GC)}$). Next, the MD ensembles of PNA conformations were used to compute the near zero bias molecular conductance (which is assumed to be directly related to the molecular CT rate)[5,30] and to analyze the distribution of computed conductance values.[6,26b] The near-zero bias conductance σ was computed using the non-equilibrium Green's function formalism and Landauer's formula,

$$\sigma = \frac{q^2}{h} \int T(E)\, F_T(E - E_F)\, dE \quad (1)$$

In eq 1, E is the energy variable, $T(E)$ is the transmission function (cf. eq 3 in the Methods section), q is the elementary charge, h is Planck's constant, and

$$F_T(E - E_F) = (1/(4k_BT))\, \mathrm{sech}^2((E - E_F)/(2k_BT)) \quad (2)$$

is the difference between the Fermi functions of the left and right electrode.[6,26b] These calculations use a Fermi energy E_F = −6.7 eV. The value of −6.7 eV is inferred from the 0.8 eV difference in the measured oxidation potential of Fc and G[8] and the −7.5 eV average HOMO energy of G resulting from CNDO calculations.[4a] Because F_T $(E - E_F)$ peaks strongly near E_F and is nearly zero elsewhere, the main contribution to the molecular conductance comes from the molecular orbitals (MOs) that lie near E_F (cf. eq 3).

Two different models were used to calculate the conductance: one that used only the nucleobases and one that used the nucleobases, the backbone, and the water solvent (see the Methods section). Figure 3 shows the calculated electronic density of states (DOS) for each of the four PNAs studied, and Table 3 shows the ratio between the median calculated conductances of aeg- and γ-PNA for each of the two studied sequences (cf. Table S4). If only the nucleobases are included in the calculations, then the DOS curves of aeg- and γ-PNA for each of the two studied sequences are very similar (Figure 3, top row). This result is consistent with the average geometries of the duplexes' nucleobase stack being similar, but the ratio between the calculated conductances of aeg- and γ-PNA nucleobase stacks does not match the experimental trends (Table 3). When the PNA backbone and water solvation shell are included in the calculation, the DOS curves of the aeg-PNAs and γ-PNAs become broad and shift with respect to each other along the energy axis (Figure 3 bottom). As a result of the shift, the aeg-PNA ensemble has more electronic states (MOs) near E_F and, consequently, larger $T(E_F)$ than the γ-PNA ensemble. The larger $T(E_F)$ translates into more MOs closer to the Fermi energy and a higher conductance for the aeg-PNAs (cf. eqs 1 and 3).

Table 3. Ratio of aeg- and γ-PNA Conductances Resulting from the Theoretical Calculations[a]

	$\sigma_{\text{aeg-PNA}}/\sigma_{\gamma\text{-PNA}}$	
sequence	bases only	whole PNA in water
$PNA_{(TA)}$	0.06 ± 0.08	1.86 ± 1.74
$PNA_{(GC)}$	0.72 ± 0.44	2.13 ± 1.83

[a]Median values for the calculated ensembles of conductances were used (cf. Figure S3B, Figure S4, and Table S4).

As shown in Table 3, inclusion of the backbone and the solvent in the calculations produces ratios between the calculated conductances of aeg- and γ-PNA that match the experimental trends well.

While it has been shown that the NA backbone does not make a significant contribution to the molecular conductance mediation,[16a,31] there are several mechanisms by which the backbone and the solvent can influence the nucleobase-mediated CT. First and foremost, the fluctuations of the backbone geometry and the positions/orientations of the solvent molecules result in fluctuations in the electric field experienced by the nucleobases. Such fluctuations cause a broadening of the MO energies of the nucleobases, estimated to be as high as 1−2 eV.[31a,32] Because the more flexible aeg-PNA produces larger electric field fluctuations than γ-PNA, it pushes more MOs toward E_F, thereby increasing $T(E)$ in the vicinity of E_F, and increasing the resulting PNA conductance (cf. eqs 1−3 and Figure S3A).

Several other mechanisms of solvent/backbone-nucleobase interaction exist, and they appear to affect the PNA MOs, DOS, and molecular conductance in different ways (Figures 3 and S3). First, the net electric field of the two backbone strands shifts the bases-only PNA DOS up the energy axis, thus increasing the PNA conductance.[32] This effect is compensated by solvent screening, which shifts the DOS curve down the energy axis (Figure S3). Second, the solvent screening apparently reduces the dipolar repulsion between the nucleobases that arises from near-alignment of neighboring nucleobases in the PNA duplex, owing to the relatively small twist of the P-type helix (17−23 deg/bp).[20b] This effect should shift the PNA DOS further down the energy axis. The cumulative result of all of these effects is a shift of the aeg-PNA DOS to higher energies than the γ-PNA DOS (Figure 3) and, consequently, a higher conductance for aeg-PNA than for γ-PNA. A detailed analysis of the relative importance of the different mechanisms of nucleobase-backbone and nucleobase-solvent interactions is beyond the scope of this paper.

The effect of backbone electric field fluctuations on the nucleobase DOS distribution represents an important new consideration for quantitative modeling of charge transport through NAs. Although it has been shown before that the CT rate in PNA is affected by backbone flexibility, those studies focused on how fluctuations affected the DNA and PNA base stack geometry and hence the base-to-base overlap and MO delocalization.[4a] In contrast, this study finds a significant difference in the CT rate for two types of PNAs that have very similar geometry and fluctuations of the nucleobase stack, as well as backbone geometry, but differ in backbone flexibility. The results presented here indicate that the backbone fluctuations may affect the nucleobase-mediated molecular conductance by an amount comparable to that arising from structural fluctuations of the nucleobases themselves (cf. Figure 3),[4a] or even nucleobase substitution (compare the average rate constants of γ-$PNA_{(GC)}$ and aeg-$PNA_{(TA)}$ in Table 2).

One should be cautious not to over-interpret the results of the theoretical calculations described here. On the one hand, the amount of solvent in the shell surrounding the simulated PNA is likely different from the amount of solvent that saturates the experimental SAMs. In addition, the length of the MD simulation (2 ns) is hardly sufficient for a comprehensive sampling of the PNA structural ensemble. It is telling that even though the experimental trends in CT rates between the aeg- and γ-PNA are reproduced here, the trends between the different PNA sequences ($PNA_{(GC)}$ vs $PNA_{(TA)}$) are not (cf. Tables 2 and S4). Such a discrepancy could be attributed to the neglect of the direct coupling between the model electrodes and the nonterminal nucleobases, including the central GC base pair where the HOMO is predominantly localized. Yet, the qualitative conclusion that larger fluctuations cause larger MO broadening and increase the PNA molecular conductance is very general and likely to be valid regardless of the computational details.

dx.doi.org/10.1021/ja301677z | J. Am. Chem. Soc. 2012, 134, 9335−9342

CONCLUSIONS

In summary, this study explored the influence of structural flexibility on the charge transfer rate constant for PNA. Both the experimental and theoretical components of this study indicate that charge transport in PNA can be suppressed by limiting the conformational flexibility of the PNA duplex, e.g., by changing the chemical nature of the backbone. While the CT occurs through the nucleobases, the fluctuations of the PNA backbone broaden the nucleobase energy levels and thus increase the CT rate constant.

METHODS

PNA Synthesis. The synthesis of PNA oligomers with C-terminal cysteine and N-terminal ferrocene moieties was previously reported and discussed;[26a,b] further details are found in the Supporting Information. Briefly, both the nonmodified and γ-modified PNA oligomers were synthesized using solid phase peptide synthesis methods with a Boc protection strategy.[15,33] Ferrocene carboxylic acid (Aldrich) was coupled to the N-terminus. Oligomers were cleaved from the resin using trifluoroacetic acid (TFA) and trifluoromethanesulfonic acid (TFMSA), precipitated in ethyl ether, and dried under nitrogen. The solid products were dissolved in aqueous solution and purified by reverse-phase HPLC. PNA oligomers were characterized by MALDI-TOF mass spectrometry on an Applied Biosystems Voyager-DE STR workstation. The observed mass of each synthesized PNA agreed well with the expected mass (Supporting Information). PNA solutions were prepared in deionized water, and the PNA concentrations were determined by UV−vis spectrophotometry assuming $\varepsilon(260)$ = 8600, 6600, 13700, and 11700 cm^{-1} M^{-1} for each T, C, A, and G monomer, respectively.[15] PNA duplexes were formed by slow cooling (from 95 C to 10 C) of solutions containing 1:1 mixtures of the complementary PNA strands.

Electrochemical Characterization of PNA SAMs. *Electrode preparation and SAM formation.* Gold ball electrodes were prepared and annealed in a manner similar to earlier reports[6,26] and were coated with PNA SAMs via 28−40 h immersion at 27 °C in 0.3−1 mL of a 20 μM PNA solution (1:1 v/v acetonitrile/pH 7.0 10 mM sodium phosphate buffer). Following incubation, electrodes were washed with deionized water and used directly in electrochemical experiments.

Electrochemical Measurements. Cyclic voltammetry (CV) was performed using a CH Instruments 618B or CHI430 electrochemical analyzer in 1 M $NaClO_4$ (pH ≈ 6−7), with a Ag/AgCl (1 M KCl) reference electrode, a platinum wire counter electrode and a PNA-modified gold wire electrode. Surface coverage was calculated by integrating the charge under voltammetric peaks. Kinetic data were obtained by plotting the peak separation versus scan rate and fitting the data by rate constants based on Marcus theory,[34] using a reorganization energy (λ) of 0.8 eV.[34b] The rate constants so determined were unchanged with a ± 0.2 eV variation in λ. Note that any changes in λ would systematically change all of measured k^0 values and the relative trends would remain the same.

Ellipsometric Measurements of PNA Film Thickness. Unmodified PNA was assembled on gold slides from EMF Corp. (Ithaca, NY) which consisted of a 100 nm Au layer over a 50 nm Ti binding layer on float glass. Gold slides for the γ-methylated PNA samples were obtained from Evaporated Coatings, Inc. (Willow Grove, PA), which consisted of a 150 nm Au layer over a 2 nm Ti binding layer on BK7 glass. The slides were cleaned by immersion in piranha solution for 2 min, and then rinsed with large amounts of deionized water, followed by ethanol rinsing and drying under nitrogen. The slides were then immersed in 1 mL of 20 μM PNA solution in 1:1 v:v acetonitrile:10 mM sodium phosphate buffer for 28 h at 27 °C. Following incubation, the samples were rinsed with ethanol and deionized water, and then dried under nitrogen. A Gaertner L-117 Null Ellipsometer was used to measure the thickness of the PNA films.

Theoretical Calculations of PNA Structure and Conductance. *Molecular Dynamics Simulations.* The initial structures of left-handed aeg-PNA duplexes $(TA)_7$ and $(TA)_3(GC)(TA)_3$ were constructed based on the average helicoidal parameters of experimentally determined aeg-PNA duplexes (PDB ID: 2K4G).[20b] The detailed protocol of initial structure construction is explained in ref 6. To generate γ-PNAs, the hydrogens atoms in the *R*-configuration at the C2′ positions along the PNA backbone were replaced with methyl groups. The force field ff99SB[35] in Amber11[36] was complemented with the previously determined atomic partial charges for aeg-[20b] and γ-methylated PNA.[25] The structures were solvated in a TIP3P water box, such that the distance between the walls of the box and the closest PNA atom was at least 17 Å. After energy minimization and equilibration, the solvated structures were subject to 2 ns of MD using the module pmemd of Amber11,[36] at T = 300 K and P = 1 atm, with periodic boundary conditions. A total of 2000 snapshots were saved every 1 ps for each trajectory and used for the subsequent electronic structure calculations. The dynamics of PNA during the simulations was characterized by the rmsd and the helicoidal parameter distribution. The RMSDs of the PNA snapshots were computed with respect to the time-averaged structure after best-fit alignment of the heavy atoms. The helicoidal parameters were computed for the PNA base pairs with 3DNA[37] (see Supporting Information).

Analysis of the Electronic Structure. The quantum mechanical analysis of the PNA structures extracted from the MD ensemble was based on single point self-consistent field calculations with the INDO/s method implemented in the CNDO program.[38] The CNDO calculations were performed for either PNA nucleobases only (capped with hydrogens), or for the complete PNA including both the nucleobases and the backbone, surrounded by water. The waters were extracted from the MD simulation for each MD snapshot and were rearranged into a Voronoi cell centered on the PNA molecule to ensure even solvation of PNA on each side (see ref 16a for detail). The water atoms were included in the CNDO calculations as point charges, assigned according to the TIP3P water model. The calculated MOs were used as input to the molecular conductance calculations.

Conductance Calculations. This work compares experimentally measured CT rates to theoretically calculated molecular conductances for different PNA molecules. The near-zero bias conductance is known to be proportional to the molecular CT rate.[5,30] Thus, using the former in lieu of the latter is valid as long as the proportionality coefficient remains the same for all the molecules studied. The coefficient of proportionality depends on the Franck−Condon DOS of the charge donor and acceptor, which includes the reorganization energy.[5,30]

The nonequilibrium Green's function (NEGF) method[39] used in our previous studies[6,26b] was employed here to calculate the molecular conductance of PNA. In the NEGF calculations, the non-hydrogen atoms of the A and T nucleobases of the terminal A:T base pairs were coupled to the virtual electrodes. The conductance σ of a given PNA structure was computed using eq 1 (*vide supra*). The transmission function $T(E)$ was determined for every PNA structure as[6,26b]

$$T(E) = \sum_m \frac{\Gamma^L_{mm}\Gamma^R_{mm}}{(E - E_m)^2 + \frac{1}{4}(\Gamma^L_{mm} + \Gamma^R_{mm})^2} + \sum_{m\neq n} \frac{\Gamma^L_{nm}\Gamma^R_{mn}}{\left[(E - E_m) - \frac{i}{2}(\Gamma^L_{mm} + \Gamma^R_{mm})\right]\left[(E - E_n) + \frac{i}{2}(\Gamma^L_{nn} + \Gamma^R_{nn})\right]} \quad (3)$$

Here, the indices m and n refer to the PNA MOs and $\Gamma^{L/R}_{mn}$ are elements of the broadening matrices $\mathbf{\Gamma}^{L/R}$ that describe the MO broadening due to the electrode coupling.[6,26b] As in refs 6 and 26b, the broadening matrix elements in this work were computed using an electrode-atom coupling strength of 0.1 eV.

ASSOCIATED CONTENT

Supporting Information

Details on PNA synthesis and duplexes melting temperatures; mass spectrometry data for the PNAs; helical parameters of the PNAs; energies of selected HOMO levels; dependence of the

PNA electronic structure on sequence and the computational model used; calculated conductance distributions.This material is available free of charge via the Internet at http://pubs.acs.org.

AUTHOR INFORMATION

Corresponding Author

dave@pitt.edu; achim@cmu.edu; david.beratan@duke.edu

Notes

The authors declare no competing financial interest.

ACKNOWLEDGMENTS

C.A., D.N.B., and D.H.W. acknowledge support from the National Science Foundation (CHE 0628169 and CHE 1059037). K.L.D. acknowledges support from a Goldblatt Fellowship during part of this research. C.A. acknowledges support by the Sloan Foundation and the Camille and Henry Dreyfus Foundation. This work used the Extreme Science and Engineering Discovery Environment (XSEDE), which is supported by National Science Foundation grant number OCI-1053575.

REFERENCES

(1) (a) Seeman, N. C. *J. Theor. Biol.* **1982**, *99*, 237−247. (b) Seeman, N. C. *Nature* **2003**, *421*, 427−431. (c) Braun, E.; Eichen, Y.; Sivan, U.; Ben-Yoseph, G. *Nature* **1998**, *391*, 775−778. (d) Liu, D.; Park, S. H.; Reif, J. H.; LaBean, T. H. *Proc. Natl. Acad. Sci. U.S.A.* **2004**, *101*, 717−722.

(2) Endres, R. G.; Cox, D. L.; Singh, R. R. P. *Rev. Mod. Phys.* **2004**, *76*, 195.

(3) (a) Uhlmann, E.; Peyman, A. *Chem. Rev.* **1990**, *90*, 543−584. (b) Núñez, M. E.; Hall, D. B.; Barton, J. K. *Chem. Biol.* **1999**, *6*, 85−97. (c) Schuster, G. B., ed. *Current Topics in Chemistry: Long Range Charge Transfer in DNA I and II*; Springer: New York, 2004; Vols. *236 and 237*.

(4) (a) Hatcher, E.; Balaeff, A.; Keinan, S.; Venkatramani, R.; Beratan, D. N. *J. Am. Chem. Soc.* **2008**, *130*, 11752−11761. (b) Liu, T.; Barton, J. K. *J. Am. Chem. Soc.* **2005**, *127*, 10160−10161.

(5) Venkatramani, R.; Keinan, S.; Balaeff, A.; Beratan, D. N. *Coord. Chem. Rev.* **2011**, *255*, 635−648.

(6) Venkatramani, R.; Davis, K. L.; Wierzbinski, E.; Bezer, S.; Balaeff, A.; Keinan, S.; Paul, A.; Kocsis, L.; Beratan, D. N.; Achim, C.; Waldeck, D. H. *J. Am. Chem. Soc.* **2011**, *133*, 62−72.

(7) (a) Nogues, C.; Cohen, S. R.; Daube, S.; Apter, N.; Naaman, R. *J. Phys. Chem. B* **2006**, *110*, 8910−8913. (b) Iqbal, S. M.; Balasundaram, G.; Ghosh, S.; Bergstrom, D. E.; Bashir, R. *Appl. Phys. Lett.* **2005**, *86*, 153901−3. (c) van Zalinge, H.; Schiffrin, D. J.; Bates, A. D.; Haiss, W.; Ulstrup, J.; Nichols, R. J. *ChemPhysChem* **2006**, *7*, 94−98. (d) Kawai, K.; Kodera, H.; Majima, T. *J. Am. Chem. Soc.* **2010**, *132*, 627−630. (e) Kawai, K.; Kodera, H.; Osakada, Y.; Majima, T. *Nat. Chem.* **2009**, *1*, 156−159.

(8) Seidel, C. A. M.; Schulz, A.; Sauer, M. H. M. *J. Phys. Chem.* **1996**, *100*, 5541−5553.

(9) (a) Meggers, E.; Michel-Beyerle, M. E.; Giese, B. *J. Am. Chem. Soc.* **1998**, *120*, 12950−12955. (b) Lewis, F. D.; Letsinger, R. L.; Wasielewski, M. R. *Acc. Chem. Res.* **2000**, *34*, 159−170. (c) Berlin, Y. A.; Burin, A. L.; Ratner, M. A. *Chem. Phys.* **2002**, *275*, 61−74.

(10) (a) Sugiyama, H.; Saito, I. *J. Am. Chem. Soc.* **1996**, *118*, 7063−7068. (b) Saito, I.; Nakamura, T.; Nakatani, K.; Yoshioka, Y.; Yamaguchi, K.; Sugiyama, H. *J. Am. Chem. Soc.* **1998**, *120*, 12686−12687.

(11) (a) Fuentes-Cabrera, M.; Sumpter, B. G.; Wells, J. C. *J. Phys. Chem. B* **2005**, *109*, 21135−21139. (b) Fuentes-Cabrera, M.; Sumpter, B. G.; Lipkowski, P.; Wells, J. C. *J. Phys. Chem. B* **2006**, *110*, 6379−6384. (c) Liu, H.; Gao, J.; Lynch, S. R.; Saito, Y. D.; Maynard, L.; Kool, E. T. *Science* **2003**, *302*, 868−871. (d) Lu, H.; He, K.; Kool, E., T. *Angew. Chem., Int. Ed.* **2004**, *43*, 5834−5836. (e) Lee, A. H. F.; Kool, E. T. *J. Am. Chem. Soc.* **2006**, *128*, 9219−9230.

(12) (a) Rakitin, A.; Aich, P.; Papadopoulos, C.; Kobzar, Y.; Vedeneev, A. S.; Lee, J. S.; Xu, J. M. *Phys. Rev. Lett.* **2001**, *86*, 3670. (b) Liu, S.; Clever, G. H.; Takezawa, Y.; Kaneko, M.; Tanaka, K.; Guo, X.; Shionoya, M. *Angew. Chem., Int. Ed.* **2011**, *50*, 1−6.

(13) (a) Kelley, S., O.; Jackson, N., M.; Hill, M., G.; Barton, J., K. *Angew. Chem., Int. Ed.* **1999**, *38*, 941−945. (b) Treadway, C. R.; Hill, M. G.; Barton, J. K. *Chem. Phys.* **2002**, *281*, 409−428. (c) Hihath, J.; Xu, B.; Zhang, P.; Tao, N. *Proc. Natl. Acad. Sci. U.S.A.* **2005**, *102*, 16979−16983. (d) Wierzbinski, E.; Arndt, J.; Hammond, W.; Slowinski, K. *Langmuir* **2006**, *22*, 2426−2429. (e) Guo, X.; Gorodetsky, A. A.; Hone, J.; Barton, J. K.; Nuckolls, C. *Nat. Nanotechnol.* **2008**, *3*, 163−167.

(14) Boal, A. K.; Barton, J. K. *Bioconjugate Chem.* **2005**, *16*, 312−321.

(15) Nielsen, P. E. *Peptide Nucleic Acids: Protocols and Applications*; Taylor & Francis: Wyndmondham, 2004.

(16) (a) Wolak, M. A.; Balaeff, A.; Gutmann, S.; Helmrich, H. J.; Vosloo, R.; Beerbom, M. M.; Wierzbinski, E.; Waldeck, D. H.; Bezer, S.; Achim, C.; Beratan, D. N.; Schlaf, R. *J. Phys. Chem. C* **2011**, *115*, 17123−17135. (b) Beratan, D. N.; Skourtis, S. S.; Balabin, I. A.; Balaeff, A.; Keinan, S.; Venkatramani, R.; Xiao, D. *Acc. Chem. Res.* **2009**, *42*, 1669−1678.

(17) (a) Koshkin, A. A.; Singh, S. K.; Nielsen, P.; Rajwanshi, V. K.; Kumar, R.; Meldgaard, M.; Olsen, C. E.; Wengel, J. *Tetrahedron* **1998**, *54*, 3607−3630. (b) Obika, S.; Nanbu, D.; Hari, Y.; Andoh, J.-i.; Morio, K.-i.; Doi, T.; Imanishi, T. *Tetrahedron Lett.* **1998**, *39*, 5401−5404.

(18) Schoning, K. U.; Scholz, P.; Guntha, S.; Wu, X.; Krishnamurthy, R.; Eschenmoser, A. *Science* **2000**, *290*, 1347−1351.

(19) Zhang, L.; Peritz, A.; Meggers, E. *J. Am. Chem. Soc.* **2005**, *127*, 4174−4175.

(20) (a) Egholm, M.; Buchardt, O.; Christensen, L.; Behrens, C.; Freier, S. M.; Driver, D. A.; Berg, R. H.; Kim, S. K.; Norden, B.; Nielsen, P. E. *Nature* **1993**, *365*, 566−568. (b) He, W.; Hatcher, E.; Balaeff, A.; Beratan, D. N.; Gil, R. R.; Madrid, M.; Achim, C. *J. Am. Chem. Soc.* **2008**, *130*, 13264−13273.

(21) (a) Bruinsma, R.; Grüner, G.; D'Orsogna, M. R.; Rudnick, J. *Phys. Rev. Lett.* **2000**, *85*, 4393. (b) O'Neill, M., A.; Becker, H.-C.; Wan, C.; Barton, J., K.; Zewail, A., H. *Angew. Chem., Int. Ed.* **2003**, *42*, 5896−5900. (c) O'Neill, M. A.; Barton, J. K. *J. Am. Chem. Soc.* **2004**, *126*, 13234−13235. (d) O'Neill, M. A.; Barton, J. K. *J. Am. Chem. Soc.* **2004**, *126*, 11471−11483.

(22) (a) Davis, W. B.; Ratner, M. A.; Wasielewski, M. R. *J. Am. Chem. Soc.* **2001**, *123*, 7877−7886. (b) Haiss, W.; van Zalinge, H.; Bethell, D.; Ulstrup, J.; Schiffrin, D. J.; Nichols, R. J. *Faraday Discuss.* **2006**, *131*, 253−264. (c) Ghosh, A. W.; Rakshit, T.; Datta, S. *Nano Lett.* **2004**, *4*, 565−568.

(23) (a) Dragulescu-Andrasi, A.; Rapireddy, S.; Frezza, B. M.; Gayathri, C.; Gil, R. R.; Ly, D. H. *J. Am. Chem. Soc.* **2006**, *128*, 10258−10267. (b) Englund, E., A.; Appella, D., H. *Angew. Chem., Int. Ed.* **2007**, *46*, 1414−1418. (c) He, G.; Rapireddy, S.; Bahal, R.; Sahu, B.; Ly, D. H. *J. Am. Chem. Soc.* **2009**, *131*, 12088−12090.

(24) (a) Brown, S. C.; Thomson, S. A.; Veal, J. M.; Davis, D. G. *Science* **1994**, *265*, 777−780. (b) Eriksson, M.; Nielsen, P. E. *Nat. Struct. Biol.* **1996**, *3*, 410−413.

(25) He, W.; Crawford, M. J.; Rapireddy, S.; Madrid, M.; Gil, R. R.; Ly, D. H.; Achim, C. *Mol. BioSyst.* **2010**, *6*, 1619−1629.

(26) (a) Paul, A.; Watson, R. M.; Lund, P.; Xing, Y.; Burke, K.; He, Y.; Borguet, E.; Achim, C.; Waldeck, D. H. *J. Phys. Chem. C* **2008**, *112*, 7233−7240. (b) Paul, A.; Bezer, S.; Venkatramani, R.; Kocsis, L.; Wierzbinski, E.; Balaeff, A.; Keinan, S.; Beratan, D. N.; Achim, C.; Waldeck, D. H. *J. Am. Chem. Soc.* **2009**, *131*, 6498−6507. (c) Paul, A.; Watson, R. M.; Wierzbinski, E.; Davis, K. L.; Sha, A.; Achim, C.; Waldeck, D. H. *J. Phys. Chem. B* **2010**, *114*, 14140.

(27) Laviron, E. *J. Electroanal. Chem.* **1979**, *101*, 19−28.

(28) (a) Anne, A.; Demaille, C. *J. Am. Chem. Soc.* **2006**, *128*, 542−557. (b) Hüsken, N.; Gębala, M.; Mantia, F. L.; Schuhmann, W.; Metzler-Nolte, N. *Chem. --Eur. J.* **2011**, *17*, 9678−9690.

(29) Skourtis, S. S.; Waldeck, D. H.; Beratan, D. N. *Annu. Rev. Phys. Chem.* **2010**, *61*, 461−485.
(30) (a) Nitzan, A. *J. Phys. Chem. A* **2001**, *105*, 2677−2679. (b) Nitzan, A. *Isr. J. Chem.* **2002**, *42*, 163−166.
(31) (a) Venkatramani, R., manuscript in preparation. (b) Tong, G. S. M.; Kurnikov, I. V.; Beratan, D. N. *J. Phys. Chem. B* **2002**, *106*, 2381−2392.
(32) Balaeff, A., manuscript in preparation.
(33) (a) Anderson, G. W.; McGregor, A. C. *J. Am. Chem. Soc.* **1957**, *79*, 6180−6183. (b) McKay, F. C.; Albertson, N. F. *J. Am. Chem. Soc.* **1957**, *79*, 4686−4690.
(34) (a) Weber, K.; Creager, S. E. *Anal. Chem.* **1994**, *66*, 3164−3172. (b) Napper, A. M.; Liu, H.; Waldeck, D. H. *J. Phys. Chem. B* **2001**, *105*, 7699−7707.
(35) Hornak, V.; Abel, R.; Okur, A.; Strockbine, B.; Roitberg, A.; Simmerling, C. *Proteins: Struct., Funct., Bioinf.* **2006**, *65*, 712−725.
(36) Case, D. A.; Darden, T. A.; Cheatham, I., T.E., ; Simmerling, C. L.; Wang, J.; Duke, R. E.; Luo, R.; Walker, R. C.; Zhang, W.; Merz, K. M.; Roberts, B.; Wang, B.; Hayik, S.; Roitberg, A.; Seabra, G.; Kolossváry, I.; Wong, K. F.; Paesani, F.; Vanicek, J.; Liu, J.; Wu, X.; Brozell, S. R.; Steinbrecher, T.; Gohlke, H.; Cai, Q.; Ye, X.; Wang, J.; Hsieh, M.-J.; Cui, G.; Roe, D. R.; Mathews, D. H.; Seetin, M. G.; Sagui, C.; Babin, V.; Luchko, T.; Gusarov, S.; Kovalenko, A.; Kollman, P. A. *AMBER11*; University of California: San Francisco, 2010.
(37) Lu, X.-J.; Olson, W. K. *Nucleic Acids Res.* **2003**, *31*, 5108−5121.
(38) Zeng, J.; Hush, N. S.; Reimers, J. R. *J. Am. Chem. Soc.* **1996**, *118*, 2059.
(39) Datta, S. *Quantum Transport: Atom to Transistor*; Cambridge University Press: Cambridge, U.K., 2005.